Frontiers in Bioscience Landmark

Front. Biosci. (Landmark Ed) **2026**; 31(3): 49970
https://doi.org/10.31083/FBL49970

Original Research

OTUB2 Mutation Promotes Thyroid Collision Tumor's Insights From the Whole-exome Sequence

Ying Xu[1,*,†], Qian Li[1,†], Mengyu Li[1,*]

[1]Department of Thyroid and Breast Surgery, Shandong Provincial Third Hospital, Shandong University, 250031 Jinan, Shandong, China
*Correspondence: xuying2205@126.com; xuying@email.sdfmu.edu.cn (Ying Xu); seaspray@163.com (Mengyu Li)
[†]These authors contributed equally.

Academic Editor: Graham Pawelec
Submitted: 17 October 2025 Revised: 13 January 2026 Accepted: 2 March 2026 Published: 19 March 2026

Abstract

Background: Thyroid collision tumors (TCTs) are rare thyroid malignancies characterized by the coexistence of distinct tumor types. We investigated the histopathology, immunohistochemistry, and gene mutations to comprehensively characterize the heterogeneity of TCTs. **Methods**: Immunohistochemistry (IHC), hematoxylin and eosin (HE) staining, and Congo red staining were performed to characterize tumor markers. DNA concentrations of all samples were measured using the Qubit DNA Assay Kit in the Qubit 2.0 fluorometer. Somatic mutations were analyzed using the Genomic Identification of Significant Targets in Cancer (GISTIC) and the NCBI-ClinVar, dbSNP, COSMIC, and HGMD databases. Bioinformatic enrichments were constructed using the Gene Ontology and Kyoto Encyclopedia of Genes and Genomes pathway databases, the OncodriveCLUST software, Cytoscape, and Circos. **Results**: Immunohistochemistry staining of papillary thyroid carcinoma (PTC) and medullary thyroid carcinoma (MTC) samples showed several distinct biomarkers. According to whole-exome sequencing, a total of 76 single-nucleotide variants (SNVs), 12 insertion–deletion variants (INDELs), and 99 copy-number variations (CNVs) were identified in the TCTs. Moreover, an OTU deubiquitinase, ubiquitin aldehyde–binding protein 2 (OTUB2), with a deletion mutation enhanced the proliferation of thyroid cancer cells in both *in vitro* and *in vivo* experiments. **Conclusion**: HRas proto-oncogene (HRAS) and STAG2 cohesin complex component (STAG2) were synchronously identified as the driver genes, while the OTUB2 deletion mutation may contribute to tumor proliferation and disease progression in TCTs.

Keywords: thyroid collision tumors; bioinformatics; OTU deubiquitinase ubiquitin aldehyde-binding 2; whole exome gene sequencing; breast cancer

1. Introduction

Thyroid collision tumors (TCTs) represent a rare pathological entity characterized by the coexistence of two distinct tumors within the thyroid gland. These tumors may comprise various histological types, including both benign and malignant lesions [1,2]. Due to the rarity of thyroid collision tumors, limited clinical data and guidelines regarding their diagnosis and treatment are available. Clinically, patients with TCTs may present with symptoms similar to those of more common thyroid disorders, such as palpable nodules, voice changes, or neck discomfort, or even hyperthyroid symptoms if the tumors produce thyroid hormones. The characteristics indicative of papillary thyroid carcinoma (PTC) can be used to identify cases through histological analysis; at the cellular level, PTC is composed of malignant epithelial cells, which exhibit features such as loss of cell polarity and an increased nuclear-to-cytoplasmic ratio [3]. Medullary thyroid carcinoma (MTC) is a rare type of thyroid cancer originating from parafollicular C cells, accounting for about 3–4% of all thyroid cancers [4]. It can occur sporadically or as a part of genetic syndromes, such as Multiple Endocrine Neoplasia type 2 (MEN2), and is often linked to mutations in the RET proto-oncogene [5]. Histopathologically, MTC is characterized by round-to spindle-shaped cells that produce calcitonin, often accompanied by amyloid deposition [6].

Cases of PTC and MTC, occurring simultaneously in the same thyroid gland are rare. Although fine-needle aspiration biopsy may be utilized to obtain cytological samples for analysis, TCTs remain difficult to diagnose. Histologically, collision tumors are typically identified and confirmed by surgical pathology, in which the distinct features of each tumor type are evaluated. This distinction is critical, as it can significantly impact treatment approaches and prognoses.

Given their rarity and complexity, TCTs remain an area of active research, necessitating further study to better understand their biological behaviour, optimal management strategies, and long-term outcomes for patients. As our understanding of these tumors evolves, increased clinical awareness may lead to improved diagnostic and treatment protocols. Our study focuses on whole-exon gene mutations of TCTs to unravel their pathogenesis, etiology, and potential therapeutic targets.

2. Materials and Methods

2.1 Clinical Samples

The tissues excised from six patients were preserved at the Pathology Department of Shandong Provincial Third Hospital, which retained the right to dispose of them. The PTC and MTC cancer tissues, comprising para-cancer tissues from the thyroid gland lobe located 1 cm from the tumor, were dissected and preserved, respectively. They were embedded in paraffin by the pathology department of Shandong Provincial Third Hospital, sectioned at 3 µm using a microtome (ARTOS 3D, Leica, Germany), and prepared for gene sequencing. Patients' consent was obtained before surgery (**Supplementary Table 1**).

2.2 Immunohistochemistry (IHC) Staining

The sections were then dewaxed, rehydrated, and subjected to antigen retrieval by heat or enzymatic methods. Primary antibodies (CD6; CD56; glycoprotein hormones alpha polypeptide (CgA); cytokeratin 1 (CK1); cytokeratin 7 (CK7); cytokeratin 19 (CK19); cis-muconate transporter protein (CT-S); Galectin-3; marker of proliferation Ki-67 (Ki67); paired box 8 (PAX8); somatostatin receptor-2 (SSTR-2); synemin (SYN); thyroglobulin (TG-S); thyroid peroxidase (TPO); transcription termination factor 1 (TTF1), 1:100 dilation; Innovation Park Drive Tucson, AZ85755, USA) specific to the target antigen were applied, followed by washing and application of secondary antibodies (Goat anti-rabbit IgG antibody, PV-9001, ZSGB-BIO company, Beijing, China; **Supplementary Table 2**). After another wash, color development was performed using DAB and, optionally, nuclear staining with hematoxylin. The sections were then mounted and covered for microscopic observation (PRECICE5122060025, Automatic Digital Slice Scanning System, Suzhou, Jiangsu, China) [7].

2.3 Hematoxylin and Eosin (HE) Staining

Tissue samples were sliced into thin sections, dewaxed in xylene, and rehydrated using a series of decreasing alcohol concentrations. The sections were stained with hematoxylin and the nuclei were stained deep blue or purple. The sections were briefly dipped in acidic alcohol to remove overstaining for differentiation. Eosin staining was performed by immersing the sections eosin, which stains the cytoplasm and other pink tissue structures. The final steps involved re-dehydration by increasing alcohol concentrations, clearing with an agent such as xylene, and mounting the sections for microscopic examination.

2.4 Whole-exome Gene Sequencing

Ten species from the carcinoma tissues (mixed with all malignant tumors), and para-cancerous normal tissues were analyzed. DNA concentration was measured using Qubit DNA Assay Kit (Thermo Fisher Scientific, Waltham, MA, USA) on a Qubit 2.0 Fluorometer (Life Technologies, CA, USA) [8,9]. Genomic DNA samples were collected and enzymatically disrupted to a size of 180 to 280 bp. The DNA fragments were then end-polished, a-tailed, ligated to a full-length adapter for Illumina sequencing, and further PCR amplified. The products were purified using the AMPure XP system (Beckman Coulter, Beverly, MA, USA) and quantified using an Agilent high-sensitivity DNA assay on the Agilent Bioanalyzer 2100 system. Clustering of the index-coded samples was performed on a cBot Cluster Generation System using the Novaseq5000/6000 S4 Reagent Kit (Illumina, San Diego, CA, USA) according to the manufacturer's instructions. Subsequently, the sequencing data were subjected to quality control analysis, including evaluation of Q30 scores and coverage depth. The data achieved a coverage depth of 100× with a total output of 12 GB, ensuring high-quality reads for downstream analysis. Raw data (raw reads) in fastq format were first processed using primary quality control. Clean reads were compared with the reference human genome (UCSC hg19) using BWA software (Wellcome Sanger Institute, Hinxton, UK), and the results were converted into the BAM format and sorted using the same tools (BerryGenomics Corporation, Beijing, China; http://www.berrygenomics.com/) [10]. The quality of the whole-exome gene sequence was confirmed by PCR-Sanger DNA sequencing, as shown in **Supplementary Fig. 1**.

2.5 Somatic Mutation and Functional Annotation

Mutect2 software 4.2.6.1 (Broad Institute, Cambridge, MA, USA) was used for variant calling and to identify somatic SNV/InDels; Enliven was used to annotate SNV/InDels. Control-FREEC software (11.6; Institut Curie, Paris, France) was used for somatic Copy number variations (CNV) detection, and ANNOVAR for somatic CNV analysis. Non-negative matrix factorization was used to decipher mutational signatures. Significantly recurrent CNV across the set of samples were determined by GISTIC analysis. The National Center for Biotechnology (NCBI)-ClinVar database, a database of single nucleotide polymorphisms (dbSNP; https://www.ncbi.nlm.nih.gov/), a catalogue of somatic mutations in cancer (COSMIC; https://cancer.sanger.ac.uk/cosmic/), and a human gene mutation database (HGMD; https://www.hgmd.cf.ac.uk) were utilized to verify the classification, genetic diversity and disease association of mutative genes which were screened from the whole-exome gene sequence testing. Sequenza software (v2.1.2; Memorial Sloan Kettering Cancer Center, New York, NY, USA) was used to detect tumor purity and ploidy.

2.6 Bioinformatics Analysis

Using HotNet2 (v1.0.1; Providence, Rhode Island, USA) software, subnetworks with significant mutations were identified to overcome the limitations of a single-gene and pathway methods, and these subnetworks showed co-

mutations across samples. Genes in the largest subnetwork in the HotNet2 analysis were enriched using Gene Ontology (GO; http://geneontology.org) and the Kyoto Encyclopedia of Genes and Genomes (KEGG; https://www.genome.jp/kegg/) analyses [11]. After filtering the MAF files to retain functional mutations, OncodriveCLUST was used to identify the driver genes. Sequenza software was used for the joint analysis of total and allelic copy number patterns to more accurately estimate tumor purity, ploidy, and precise genotypes of copy number alterations. SciClone software (Stanford, CA, USA) was used to identify the number and genetic composition of the subclones. Visualized diagrams were accessed using the Xiantao database (https://www.xiantaozi.com).

2.7 Protein-protein Interaction Analysis

After the significantly mutated genes were identified, the STING database (https://cn.string-db.org/) was used to explore protein-protein interactions (PPI), and Cytoscape software 3.10.1 (La Jolla/San Diego, CA, USA) was used to visualize the PPI data and screen the hub genes.

2.8 Driver Gene and Advanced Analysis

The Cancer Genomic Census Database and Oncology Knowledge Base database were used to screen driver genes in TCT. The OncodriveCLUST tool (Institute for Research in Biomedicine, Barcelona, Spain)was used to analyze and visualize the proportions of driver genes.

2.9 Cell Culture

Nthy-ori-3.1 cell-line (ZQ0874, Zhongqiaoxinzhou cell company, Shanghai, China), TPC-1 (ZQ0875, Zhongqiaoxinzhou cell company, Shanghai, China) and TT (ZQ0232, Zhongqiaoxinzhou cell company, Shanghai, China) cell-lines were purchased and cultured in Dulbecco's modified Eagle medium supplemented with 10% fetal bovine serum (Biological Industries, Kibbutz Beit HaEmek, Israel) in the presence of penicillin, streptomycin and L-glutamin (Corning, New York, NY, USA) at 37 °C, 5% CO_2 humidified conditions. All cell lines were validated by STR profiling and tested negative for mycoplasma contamination.

2.10 Transient Transfection

Detailed information on OTUB2 was found in the NCBI database (Gene ID: 78990; GRCh38.p14; https://www.ncbi.nlm.nih.gov/datasets/gene/78990/). For transient transfection, TPC-1 and TT cells were seeded at 1×10^6 cells/well in 6-well plates. Transfections were performed using Lipofectamine 2000 at 85% confluency, following the manufacturer's protocol, and incubated for 48 hours in DMEM (10% FBS, 1% P/S) at 37 °C, 5% CO_2. Mixed liquors, including Lipofectamine 2000 and 4 µL plasmids (pcDNA3.1 + OTUB2-DELETION MUTATION; Plvx-siRNA2-Puro + OTUB2-DELETION MUTATION; Tsingke Biological Technology, Beijing, China), were added into cell plates for 6 hours with antibiotic-free medium, and the cells were cultured for a further 48 hours.

2.11 Cell Wound Healing Assay

Cells were seeded at 1×10^6 cells/well in 6-well plates and incubated in RPMI-1640 (10% FBS) until they achieved 95–100% confluency. Sterile 200 µL pipette tips were used to create three linear wounds per well perpendicular to plate markers. Detached cells were removed by gentle PBS washing (Ca^{2+}/Mg^{2+}-free). Wells were replenished with serum-free medium containing test compounds. Phase-contrast images (4 × objective) were captured at 0/48/72 hours at identical coordinates using an Olympus IX73 microscope (Olympus Corporation, Center Valley, PA, USA). Migration distance was quantified as: [\text{Migration distance(µm)}=\frac{\text{Wound-width}{0h}-\text{Wound-width}{t}} {2}] using Image J (National Institutes of Health, Bethesda, MD, USA) with the "MRI Wound Healing" macro. Three technical replicates per condition were analyzed.

2.12 Flow Cytometry

Apoptosis detection used Annexin V-FITC (5 µL; BioLegend, 640945) and PI (2 µg/mL) in calcium-containing binding buffer (10 min RT, dark). Samples were analyzed on a BD FACS Celesta (BD Biosciences, San Jose, CA, USA), collecting ≥10,000 viable events (FSC/SSC-gated).

2.13 Monoclonal Proliferation Assay

After preparing a single-cell suspension, thyroid cancer cells were seeded at a density of 200 cells per well in 6-well plates containing 2 mL of RPMI-1640 medium supplemented with 10% FBS and 1% penicillin/streptomycin. Then, they were incubated at 37 °C with 5% CO_2 for 24 hours to ensure attachment. The cultures were undisturbed for 14 days and the medium was replaced every 3 days with prewarmed, fresh medium. Colonies were fixed with 4% paraformaldehyde for 15 minutes at room temperature, stained with filtered 0.5% crystal violet solution for 30 minutes, rinsed gently with ddH_2O, and air-dried on plates. Colonies containing ≥50 cells were quantified using a stereomicroscope (Carl Zeiss AG, Jena, Germany), with plating efficiency calculated as (number of colonies / 200) × 100%.

2.14 In Vivo Model Construction

Five-week-old female nude mice (BALB/c, Weitonglihua company, Beijing) were used for the animal experiments, with at least five mice per group. To construct the sub-axillary transplantation, 100 µL of PBS containing 1×10^6 cells (TPC-1, TT-OTUB2-MUTATION, TPC-1-OTUB2-MUTATION) from distinct groups was injected into the right axilla of nude mice. Ten days later, the tumor was measured by a scaleplate, and the mice were

sacrificed on day 28. The original tumors were measured every three days for a total of seven measurements. We ensured that all animals received humane care in conditions of 24 °C and 35% humidity, and they were free to eat and drink. The sacrificed animals were anesthetized with low-concentration isoflurane (5%) delivered in oxygen, followed by maintenance under a capsule for five minutes, and then with high-concentration isoflurane for ten minutes (6.5% with 4.5 mL/min oxygen flow rate; No, CAS26675-46-7, Chemical Book Company, Hebei, China). Deep surgical anesthesia was confirmed by the absence of a pedal withdrawal reflex and the loss of corneal reflex. Subsequently, while the animals were under this deep plane of anesthesia, euthanasia was performed immediately by rapid cervical dislocation. The animal study was approved by the Shandong Provincial Third Hospital Committee on Laboratory Animal Issues (No, DWSY-G2024005). This study was carried out in accordance with the ARRIVE guidelines (https://arriveguidelines.org).

2.15 Statistical Analysis

SPSS 28.0 version (IBM Corp., Chicago, IL, USA) analyzed all data in this study and each experiment was repeated at least 3 times. Student's *t*-test was used to compare microarray data and two groups of data, while the mean $\pm$ standard deviation (SD) was used for all numerical results. For multiple-group comparisons, the data distribution was assessed to determine whether parametric or non-parametric tests were appropriate. When assumptions of normality and homogeneity of variance were met, one-way analysis of variance (ANOVA) was performed to evaluate overall differences, followed by Tukey's post hoc test for pairwise comparisons to control the family-wise error rate at $\alpha = 0.05$. Three independent replicates were performed for each experimental condition. Some graphs were generated using GraphPad Prism 9.0 software (San Diego, CA, USA) ($*p < 0.05$, $**p < 0.01$, $***p < 0.001$, $****p < 0.000$).

3. Results

3.1 One of Six Patients' Clinical Information

A 62-year-old Chinese woman suffering from neck discomfort visited a standard hospital and underwent thyroid examination using ultrasound on June 12, 2023. She had no chronic diseases or family history of thyroid tumors, and did not have any harmful habits, such as smoking or alcohol consumption. Ultrasonography revealed multiple nodules in the bilateral thyroid lobes, the largest of which measured 1.7 $\times$ 1.4 cm in the right thyroid lobe (Fig. 1A–F). The mass was classified as "4b" according to the protocol of the Thyroid Imaging Reporting and Data System Protocol. Then, preoperative FNA cytology was performed on the isthmus node, and the cytological result was diagnosed as "PTC" under Category VI of the Bethesda system. No distant metastases were detected during preoperative examinations. Subsequently, the patient underwent a total thyroidectomy via thoracoscopy with central lymph node dissection. The patient recovered well and has been in good health since the surgery.

3.2 Pathological Presentation

On gross examination after the operation, the specimen measured 5.5 $\times$ 4.2 $\times$ 1.3 cm, containing three tumors. The larger tumors (right lobe), measuring 1.8 $\times$ 1.4 cm and presenting a yellowish and grey mass, were diagnosed as an "MTC" (Fig. 1G). The other tumors (0.4 $\times$ 0.4 cm and 0.6 $\times$ 0.8 cm) in the isthmus and left portion, presenting off-white and quasi-circular nodes, were diagnosed as "PTCs" (Fig. 1H). At this point, the patient was diagnosed with TCT. The peripheral tissues around the tumors were diagnosed as follicular nodular lesions, and neither necrosis nor hemorrhage was observed. PTC and MTC specimens were staged as pT1aN0M0 and pT1bN0M0, respectively, according to the American Joint Committee on Cancer 8th edition criteria.

Several biomarkers for IHC and HE staining were performed to determine the diversity of the PTC and MTC. This indicated that the PTC showed a bluish-violet change (Fig. 1I). At the same time, MTC showed cytoplasmic calcitonin immunoreactivity and showed a light pink colour under Congo staining (Fig. 1J,K). Normally, the IHC staining for PTC is positive for CK19, Galectin-3, and MC, but negative for CD56, TPO, CT, CgA, SYN, and PTH. In contrast, the IHC staining also revealed that the MTC was positive for TTF1, SYN, CT, SSTR-2, CK-19, CK-7, CK-1, and CD56, while it was negative for TPO, TG, PAX-8, and Galectin-3 (Fig. 1L–X; **Supplementary Table 3**), suggesting that MTC was more heterogeneous than the PTC (**Supplementary Fig. 2**). In addition, the Ki-67 value in the MTC was 3%, suggesting that MTC cells had low proliferation. Positivity for CD56, TTF1, and SYN was associated with cell proliferation, migration, signal transduction, and disease progression (**Supplementary Table 4**).

3.3 Single Nucleotide Polymorphism Analysis

In accordance with the gene mutations in all groups, we found that gene mutations in the MTC were worth paying attention to, compared to the lack of special gene mutations in the PTC. Exon genes in TCT tissues exhibit non-isotropic somatic mutations, including Single nucleotide variants (SNVs), Insertion and deletion (INDEL), and Copy number variations (CNVs). In total, 23 mutations were found in the exonic regions of the DNA sequences, and 27 out of 76 SNV genes were found to be disease-associated mutations in MTC tissues (Fig. 2A,B; **Supplementary Tables 5,6**). And the SNP mutations of PTC tissues were also shown with compared heatmap and bar graphs (**Supplementary Fig. 3A–D**).

Subsequently, cell components, molecular functions, and signaling pathways were illustrated using GO/KEGG

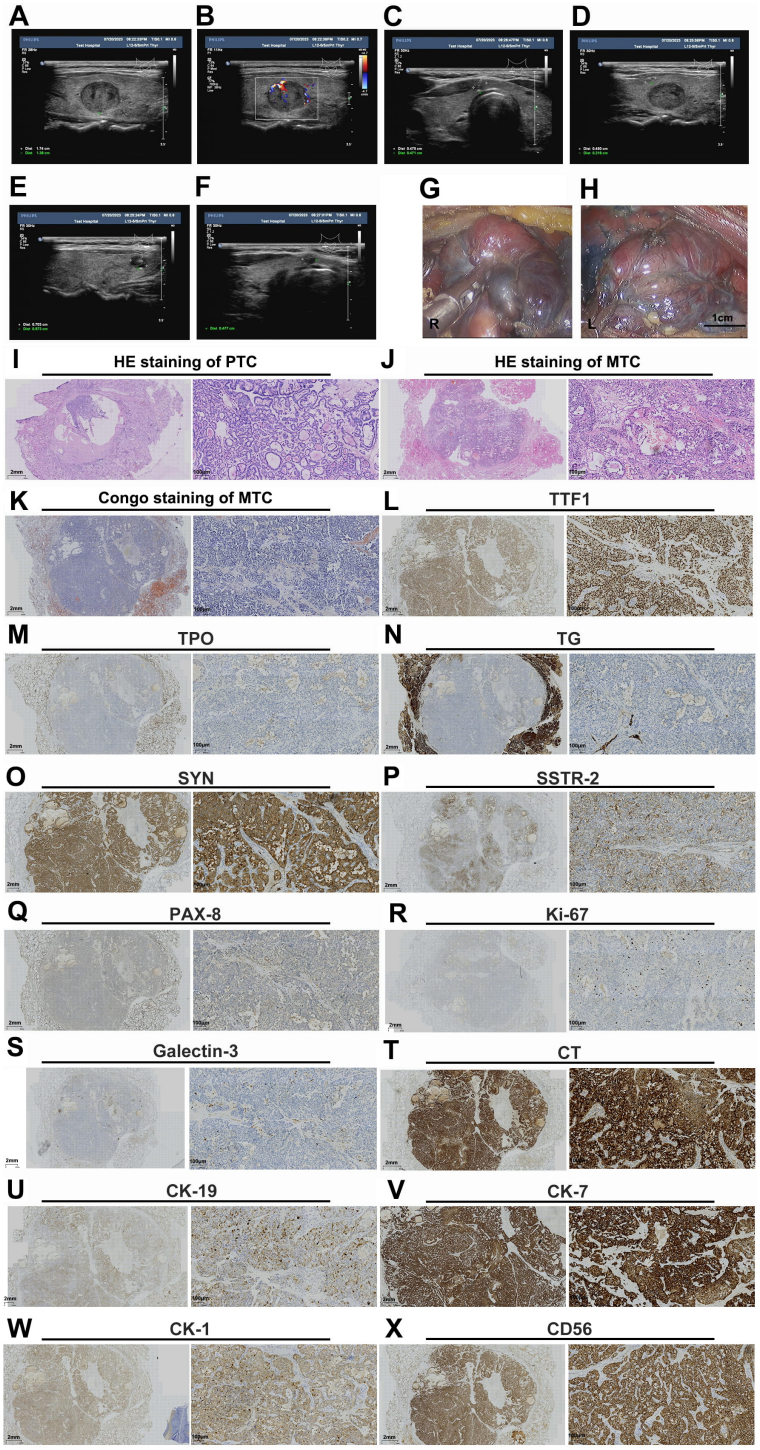

Fig. 1. Ultrasound images and operation process of thyroid collision tumor with immunohistochemistry stainings. (A,B) A 1.74 × 1.38 centimeter gross thyroid right lobe was noted on ultrasonography, with abundant blood flow signals. (C) A 0.475 × 0.471 centimeter nodule was found adjacent to the air tube. (D–F) Another node was also discovered measuring 0.450 × 0.218 centimeter, 0.703 centimeter, and 0.477 centimeter in the thyroid, respectively. (G,H) The right lobe and the left were excised under the endoscope. The scale bar is 1 cm. (I) HE staining showed classical papilliform structures of papillary carcinoma of TCT. (J,K) Congo red or HE stains can be employed to detect the medullary carcinoma components of TCT. (L–X) The IHC showed positive or negative staining for medullary carcinoma markers. The scale bar is 2 mm and 100 µm. HE, hematoxylin and eosin; TCT, thyroid collision tumor; IHC, immunohistochemistry; PTC, papillary thyroid carcinoma; MTC, medullary thyroid carcinoma; TTF1, transcription termination factor 1; TPO, thyroid peroxidase; TG-S, thyroglobulin; SYN, synemin; SSTR-2, somatostatin receptor-2; PAX8, paired box 8; Ki67, marker of proliferation Ki-67; CK, cytokeratin; CD, cytotoxic T-lymphocyte associated protein 4.

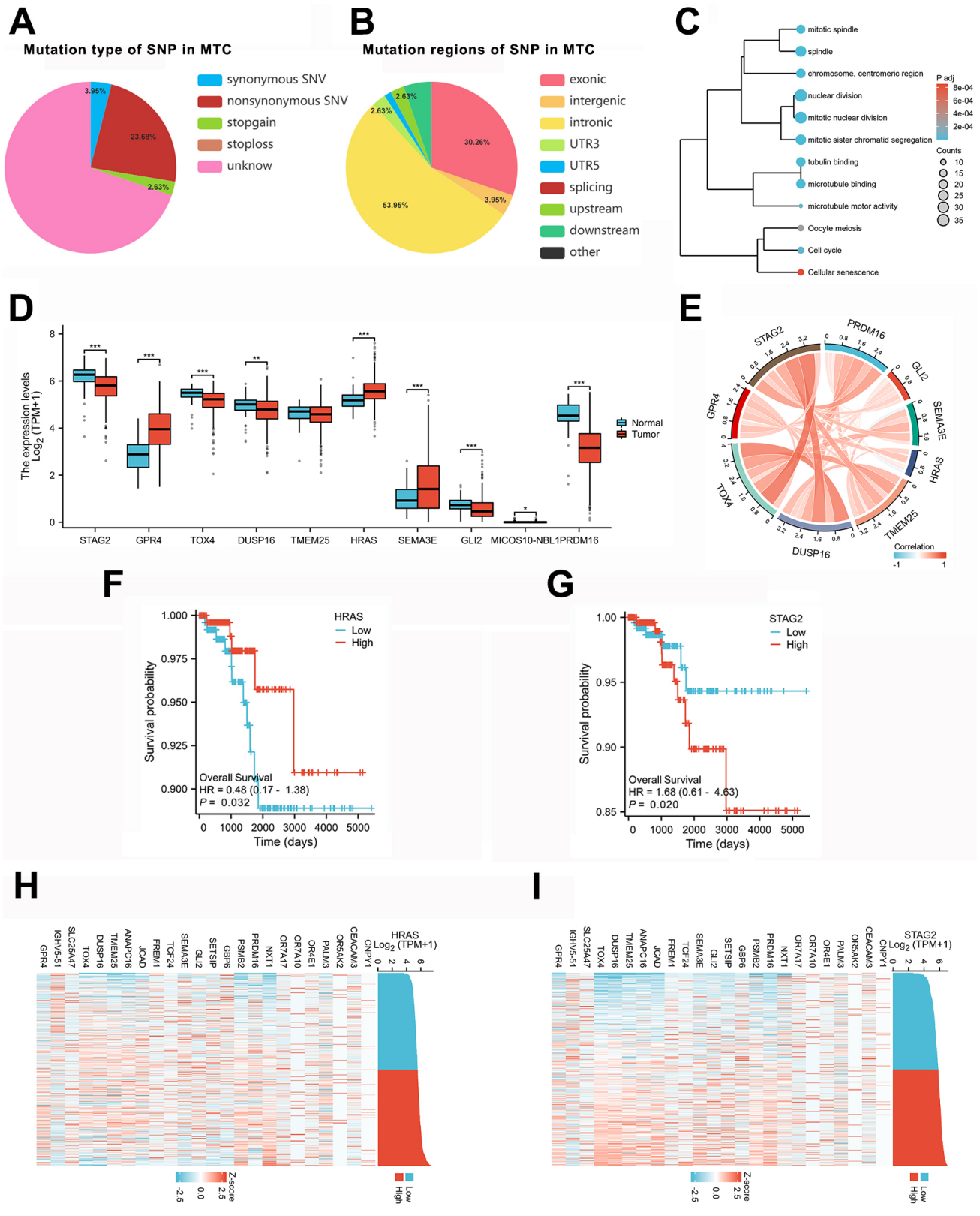

Fig. 2. Single-nucleotide variants were screened for gene mutation type, and bioinformatics analyses of significant mutative genes were performed. (A,B) The proportion of mutation types and regions of SNV. (C) Seventy-six SNV genes were enriched by GO/KEGG database visualizations. (D) The expression of cancer-associated SNV genes in the normal and tumor tissues was shown. (E) The chord diagram predicted a correlation coefficient among them. (F,G) Overall survival curves of HRAS and STAG2 in patients with thyroid carcinoma. (H,I) The correlation heat map of HRAS and STAG2 in thyroid carcinoma. SNV, single nucleotide variant; HRAS, HRas proto-oncogene; STAG2, STAG2 cohesin complex component. *$p < 0.05$; **$p < 0.01$, ***$p < 0.001$.

enrichments to provide bioinformatic insights into the aforementioned significantly mutated genes in TCTs (Fig. 2C; **Supplementary Fig. 3B**; **Supplementary Fig. 3E**). The Venn graph helps us to find out the co-mutation SNP genes of TCTs, verifying thirteen genes (**Supplementary Fig. 3F**). Deeply analyzing, MINOS1-NBL1, PRDM16, GLI2, SEMA3E, TMEM25, DUSP16, TOX4, and GPR4 were involved in the progression and prognosis of multiple malignant tumors. In contrast, HRAS and STAG2 were identified as cancer driver genes by the OncodriveCLUS tool both in the MTC and PTC tissues, suggesting that these distinct mutations may contribute to TCT tumorigenesis (**Supplementary Fig. 4A**). Expression of GPR4 and SEMA3E was higher in thyroid tumors than in normal thyroid tissues, according to the TCGA database. In contrast, another thyroid cancer-associated mutated gene was lower in thyroid tumors than in normal thyroid tissues (Fig. 2D), demonstrating that GPR4 and SEMA3E participate in cell proliferation and cellular senescence. The chord diagram indicated a high correlation between STAG2 and TOX4 (Fig. 2E), suggesting that these genes may regulate tumorigenesis in a complex manner. Additionally, STAG2 was associated with poor overall survival in patients, but HRAS expression had the opposite effect (Fig. 2F,G). Further analysis revealed that the two driver genes were co-expressed with other SNP mutative genes (Fig. 2H,I).

3.4 Insertion and Deletion Analysis

The INDEL mutative genes were found in TCTs, 33.33% of which occurred in the exon section, and 41.67% of which occurred in the intronic section of MTC tissues (Fig. 3A–C); meanwhile, in PTC tissues, there were 5.01% in the exon section and 21.73% in the intronic section (**Supplementary Fig. 4B,C**). The chemokine receptor binding and intermediate filament binding functions of NES, BCL2L14, OTUB2, and CEACAM3 were clustered using the GO/KEGG database (Fig. 3D,E; **Supplementary Fig. 4D**), indicating that these genes were related to protein ubiquitination. Furthermore, CEACAM3 expression was not significantly different between tumors and normal thyroid tissues, whereas low-level expression of BCL2L14 and OTUB2 showed statistical significance in distinguishing tumor stages (Fig. 3F,G). The chord diagrams, presenting PPI networks for four genes, were analyzed separately and showed that BCL2L14 had fewer interactions with other genes (Fig. 3H). Furthermore, in terms of AUC, OTUB2 showed a higher AUC than the other three genes (Fig. 3I), and low OTUB2 expression was associated with a lower long-term survival rate, suggesting that OTUB2 might be a protective factor in thyroid cancers (Fig. 3J). Additionally, OTUB2 was the co-mutation INDEL gene both in MTC and PTC tissues (**Supplementary Fig. 4E**). Finally, a visual simulation diagram displayed the INDEL variation process (Fig. 3K).

3.5 Copy Number Variations Analysis

Euchromosomes and the sex chromosome X both harbored CNV genes, comprising more than 300 mRNA, lncRNA, and microRNA genes (Fig. 4A; **Supplementary Table 7**; **Supplementary Fig. 5**). The PPI network and hub genes were enriched using the Sting database and Cytoscape software, suggesting that miR-663a and CEP290 were identified as novel hub genes in the TCT, implying that miR-663a, as the critical node, might construct a "ceRNA" network to reveal potential molecular mechanisms in the development and process of TCT (Fig. 4B,C). The driver genes HRAS and STAG2 had T>C missense mutations on chromosome 11 and an A>T mutation on chromosome X, both belonging to the SNP variant type (**Supplementary Table 3**). The CCF of significantly mutated genes was listed to identify the top five genes: GALNT4, TOX, TMEM25, CST8, and STAG2 (**Supplementary Table 8**). The Circos graph displays whole gene mutations in the TCTs, and the structured flowchart summarizes the main content of our study (Fig. 4D,E; **Supplementary Fig. 5**), presenting the logical scanning of mutated genes. Furthermore, Circos plots were utilized to depict a panoramic view of gene mutations, effectively illustrating their distribution and patterns across the genome.

3.6 OTUB2-deletion Mutation Promoted Cancer Proliferation

Based on the above bioinformatics analysis and the hypothesis that OTUB2 serves as a protective tumor marker, we will conduct both *in vivo* and *in vitro* experiments to verify the impact of OTUB2 gene mutation-induced low OTUB2 protein expression on the phenotypic characteristics of thyroid cancer cells. Then, we constructed plasmids harboring the OTUB2 deletion mutant (-CCCCA-). These constructs were transfected into the appropriate PTC (TPC-1) and MTC (TT) cell lines, with normal thyroid epithelial cells (Nthy-ori-3-1) serving as references. The expression of proliferation markers CDK4 and Ki-67 was assessed using quantitative PCR and Western blot. The results demonstrated significantly lower basal OTUB2 expression in both TT and TPC-1 cells compared to Nthy-ori-3-1 cells. Notably, OTUB2 depletion markedly enhanced the expression of CDK4 and Ki-67 in both carcinoma cell lines (Fig. 5A–G). Consistent with these findings, flow cytometric analysis of apoptosis and colony formation assays revealed that OTUB2 deletion significantly suppressed apoptosis (Fig. 5H,I). A 48-hour wound healing assay further indicated enhanced migratory capacity in OTUB2-depleted cancer cells (Fig. 5J,K). *In vivo* subcutaneous xenograft models in nude mice showed that tumors derived from OTUB2-depleted MTC (TT) cells were significantly larger than those from wild-type TPC-1 cells and even OTUB2-depleted TPC-1 cells (Fig. 5L–N). These collective results suggest a more pronounced oncogenic role of OTUB2 depletion in TCTs.

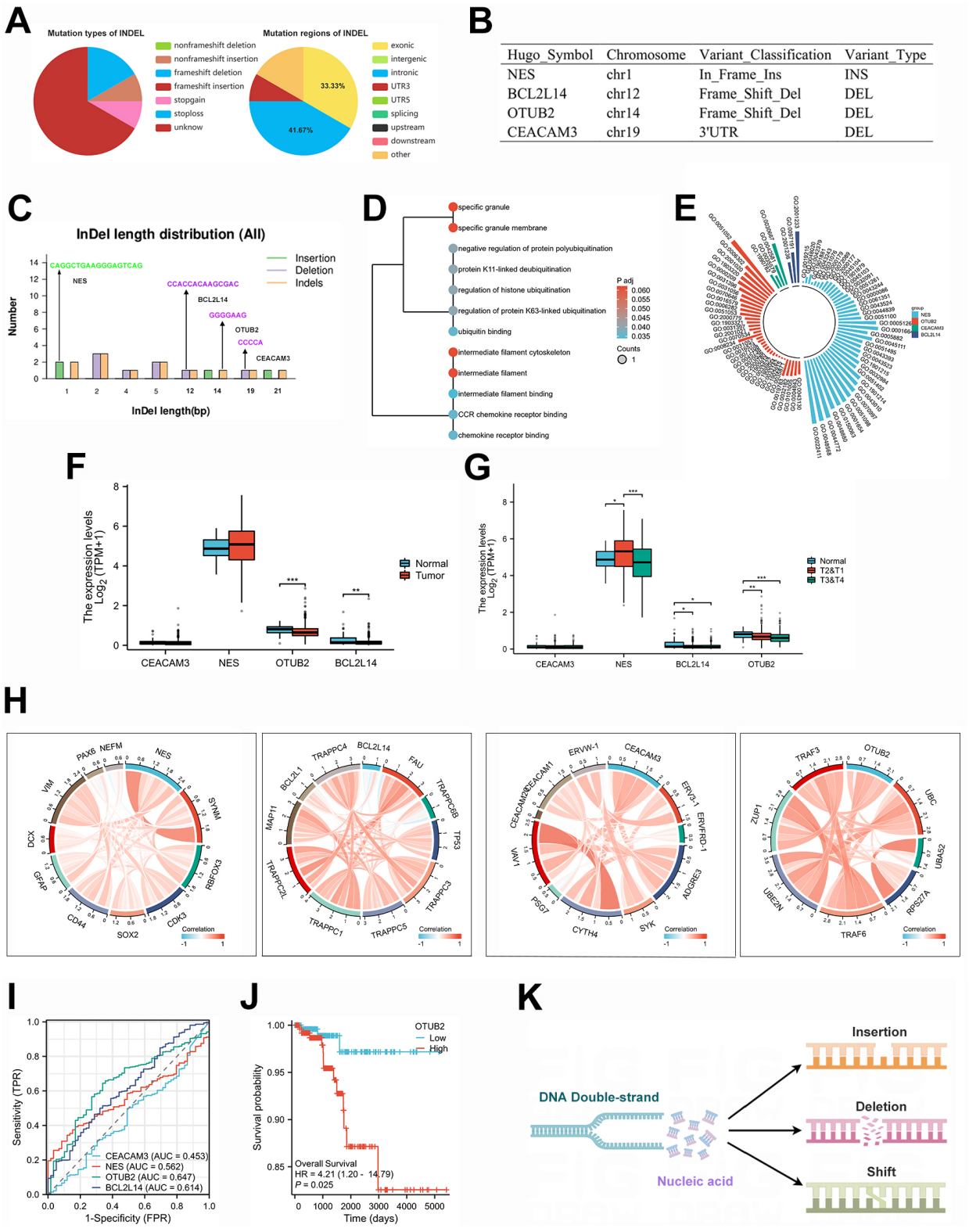

Fig. 3. The INDEL mutation type was screened, as were bioinformatics analyses of significant mutative genes. (A) The proportions of mutation types and INDEL regions. (B,C) There were four significant INDEL genes with determinate mutative sequences in distinct chromosomes. (D,E) GO/KEGG database visualizations of INDEL genes. (F,G) INDEL gene expressions in the normal and thyroid tumor tissues, as well as those of T stages. (H) PPI networks and correlation chord diagrams of INDEL genes. (I) ROC curves of INDEL genes. (J) The high expression of OTUB2 was correlated with poor OS of patients with thyroid carcinoma. (K) The simulated diagram of the INDEL process in DNA sequences. INDEL, insertion and deletion variants; ROC, receiver operating characteristic. *$p < 0.05$; **$p < 0.01$, ***$p < 0.001$.

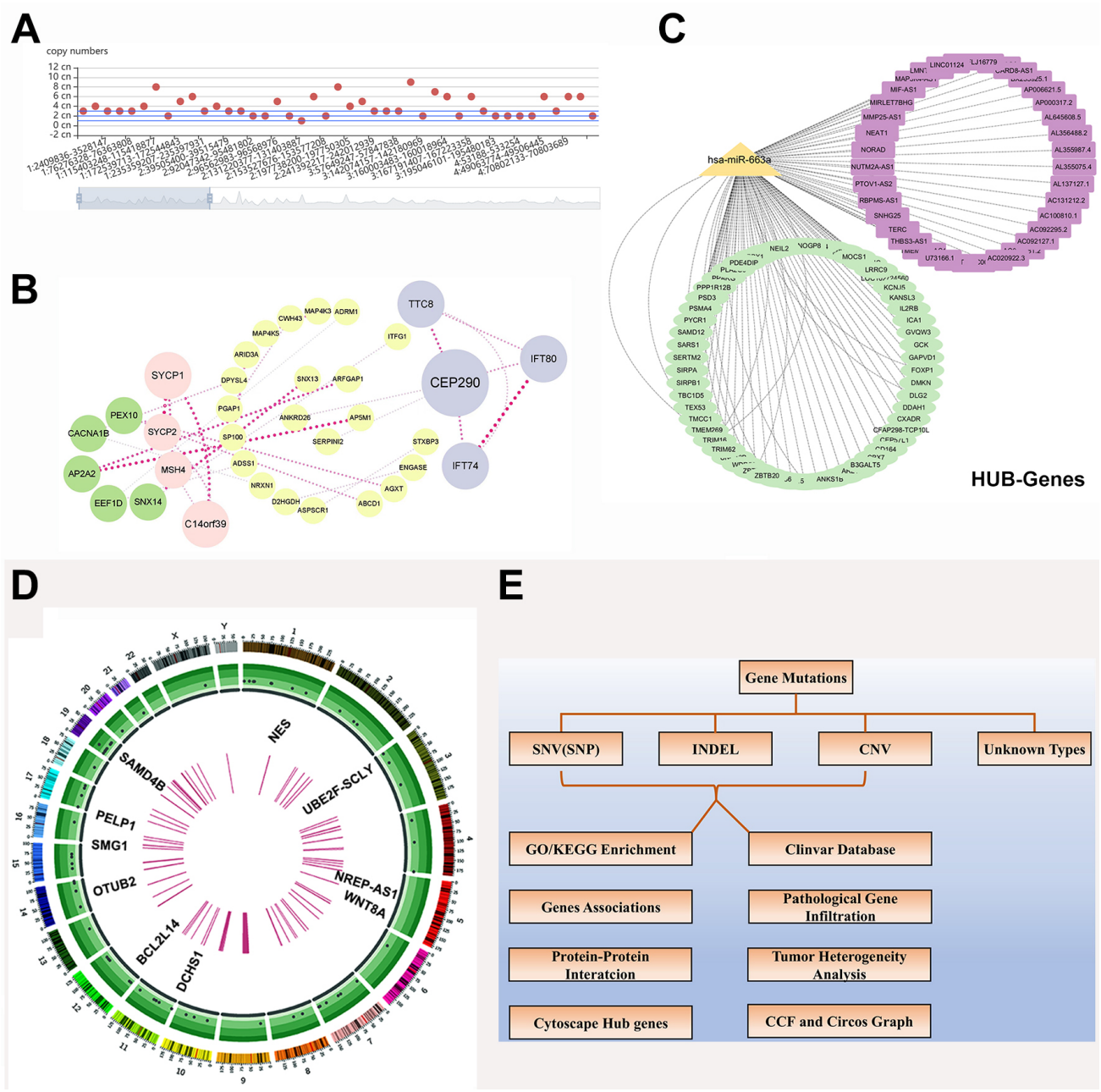

Fig. 4. Bioinformatics information of CNV genes and advanced analysis of whole-exome mutation genes. (A) The number and position of CNV genes. (B) Hub genes were identified from approximately 200 CNV genes using Cytoscape software. (C) CNV miR-663a, as a central node, constructed a "ceRNA" network. (D) Circos graph of the whole-exome mutation in MTC. (E) Flow chart of the procedures of our study. CNVs, Copy number variations.

4. Discussion

TCT is a rare phenomenon in which two distinct histological tumor types coexist within the thyroid gland without intermingling. These tumors are often juxtaposed with each other while maintaining separate identities. Understanding the molecular and genetic characteristics of TCT is crucial for developing targeted therapies and improving diagnostic accuracy. From a histopathological perspective, a TCT consists of two components: PTC and MTC, PTC and FTC, or PTC and oncocytic carcinoma (OTC) [1,12,13]. The poorest overall survival with TCT was observed in cases featuring the coexistence of papillary and oncocytic cancers, with one patient surviving only 14 months [13]. However, the patient who underwent TCT excision in our study remains alive and free of metastasis, indicating a good prognosis. Furthermore, in terms of the Kawasaki's report [12], the Ki-67 ratio in FTC was only 3% compared to 5% in PCT, a finding similar to ours. However, Kawasaki analyzed only CK-1, TTF-1, TG, CK19, Galectin-3, and Ki-67 via IHC staining; by comparison, in addition to single mu-

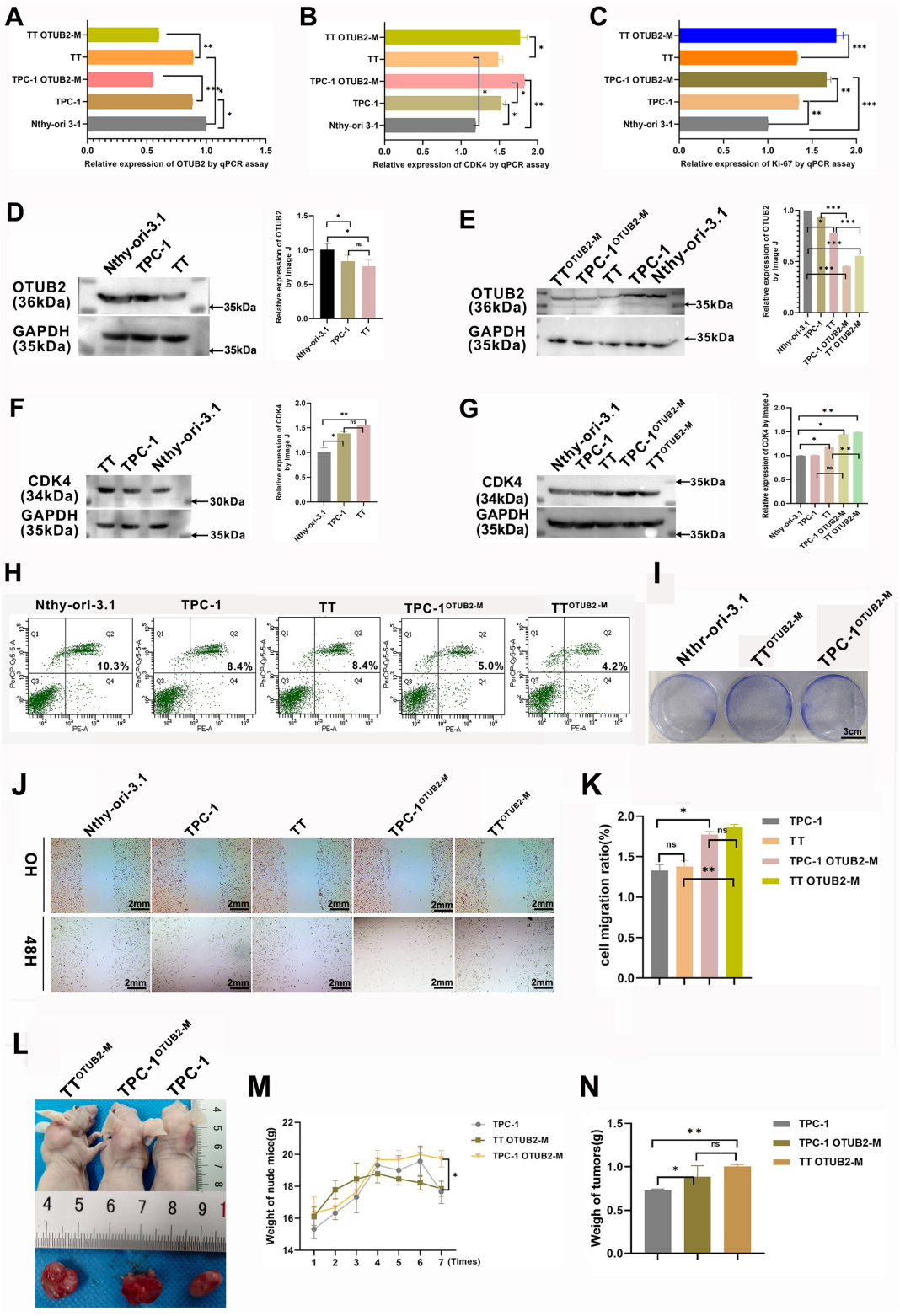

Fig. 5. The OTUB2 deletion mutation promoted the proliferation of cancer cells. (A–C) The OTUB2 and proliferative markers were detected by qPCR assay; (D–G) the OTUB2 and CDK4 expression were measured by Western blot assay; (H) the apoptosis ration in Nthy-ori-3.1 cells and thyroid cancer cells were shown by flow cytometry assay; (I) cell colon experiments in Nthy-ori-3.1 and thyroid cancer cells treated with OTUB2-deletion mutation plasmids. The scale bar is 3 cm; (J,K) the wound healing area in Nthy-ori-3.1 cells and thyroid cancer cells. The scale bar is 2 mm; (L–N) the thyroid tumors and weights of tumors and nude mice were measured by the subcutaneous transplanted tumor model with three type of thyroid cancer cells (n = 5/per group). *$p < 0.05$; **$p < 0.01$; ***$p < 0.001$; ns, non-statistical significance.

tative gene detection, we enlarged the scope of IHC staining and implemented whole-exome gene sequencing to retrieve extensive mutative gene information from TCTs. We not only explored the SNV mutations of HARS and STAG2 as the cancer driver genes, but also categorized the pivotal In-Del mutations of OTUB2, considering as a factor of molecular mechanism in MTCs.

Genetic testing is a pivotal method for unveiling the heterogeneity of cancer cells, especially regarding genetic mutations. The BRAF (V600E) mutation, affecting 35–80% of PTC cases and 40% of FTC cases, leads to a change at the 600th codon from valine to glutamate, resulting in persistent BRAF activation [14]; this was also observed in the PTC tumors examined in this study. Conversely, RAS mutations, notably NRASQ61R, occur in 40–60% of MTCs and 20–40% of follicular adenomas and play a pivotal role in the emergence of these and other cancers [15], consistent with our results.

When a TCT is identified in histological examination, it is imperative to perform a comprehensive pathological assessment that includes both morphological examination and genetic analysis, with a particular emphasis on detecting multiple gene mutations. Notwithstanding this, numerous articles have elucidated multiple mutative genes in the independent carcinomas of thyroid tumors, but there are no reports of gene variations in TCTs identified using whole-exome gene sequencing technology. Therefore, our study represents the first exploration of a Chinese patient with concurrent PTC and MTC. HRAS and STAG2 were identified as the driving genes, whereas the INDEL mutation-OTUB2 was found to be involved in the proliferation of TCTs, contributing to poor outcomes [16,17]. According to recent reports, OTUB2 was associated with the growth of liver cancer and invasion of PTC by suppression of the NF-kappaB signaling pathway [18]. Furthermore, OTUB2 was also found to contribute to vascular calcification in chronic kidney disease and deubiquitinated RIPK3 in neuronal necroptosis after ischemic stroke [19,20]. As such, OTUB2 should be subject to in-depth investigation in cases of MTC, FTC, and TCTs.

Next, we successfully constructed a “ceRNA” network via the mutative node-miR-663a, combining upstream LncRNAs with downstream target mRNAs. This network may play a pivotal role in elucidating the causal mechanisms underlying TCT. MiR-663a is involved in the process, development, and progression of lung cancer [21], hepatocellular carcinoma [22], breast cancer [23], renal cell carcinoma [24], and osteosarcoma [25], but its function under normal or mutated conditions in TCTs remains uncertain.

While emerging evidence has established OTUB2 as an oncoprotein in multiple cancers through its deubiquitinating function [26], our study focused on its role in thyroid cancer by constructing a deletion mutation (removal of the “-CCCCA-” sequence) via site-directed mutagenesis of a wild-type OTUB2 cDNA template in a mammalian expression vector. Our findings reveal that depletion of OTUB2 in thyroid cancer models enhances proliferation, survival, and migration, contrasting with its established oncogenic role in cancers such as colorectal and breast, where OTUB2 overexpression stabilizes clients, such as c-Myc and AKT, to drive progression [26,27]. OTUB2 depletion had the strongest tumorigenic effect in MTC-derived cells. This finding crucially illustrates the functional heterogeneity between the different components of the collision tumor. Notably, in cancers such as colorectal and breast, OTUB2 typically acts as an oncoprotein by deubiquitinating and stabilizing key drivers like c-Myc and AKT, thereby promoting proliferation and survival. Similarly, in glioblastoma, OTUB2 stabilizes EGFR and modulates DNA damage response to fuel tumor growth, while in hepatocellular carcinoma, it facilitates metastasis by stabilizing Snail1 to drive epithelial-mesenchymal transition [28,29]. Our findings reveal a context-dependent, tumor-suppressive role for OTUB2 in thyroid cancer, which contrasts sharply with its well-established oncogenic functions in several other malignancies, underscoring critical tissue-specific mechanisms. In stark contrast, our study demonstrates that OTUB2 depletion in thyroid cancer models—particularly in medullary thyroid carcinoma (MTC)—enhances proliferation, migration, and tumorigenesis. This divergence highlights that OTUB2’s function is not universal but is shaped by tissue-specific interacting partners, signaling contexts, and mutational backgrounds. For instance, thyroid-specific substrates or pathway crosstalk (e.g., unique RAS/MAPK dynamics in MTC) may redirect OTUB2 toward stabilizing tumor-suppressive networks rather than oncogenic clients. Thus, while OTUB2 is largely oncogenic in epithelial-derived carcinomas outside the thyroid, it appears to fulfill a protective, context-dependent role in thyroid carcinogenesis—a distinction that urges careful re-evaluation of its mechanistic contributions across different tissue types.

Additionally, based on KEGG enrichment highlighting pathways like MAPK signaling and protein processing, we hypothesize a mechanistic model where mutated STAG2 induces chromatin instability, potentiating HRAS/MAPK-driven oncogenic transcription and proliferation. The loss of OTUB2, a deubiquitinase, fails to degrade key pathway components (RAS), further amplifying this signal and accelerating tumor progression in the collision tumor. This creates a synergistic oncogenic network.

5. Limitations

This study has several limitations that should be considered when interpreting the results. First, due to the rarity of TCTs, our single-center cohort consisted of a limited number of patient samples. This restricted sample size may reduce the statistical power to detect low-frequency co-mutated genes, potentially leading to an incomplete molec-

ular profile of TCTs and overlooking shared genetic drivers. Second, *in vitro* and *in vivo* experiments were conducted using established PTC and MTC cell lines separately, which do not recapitulate the potential interactions or mutual influences between the two cancer types within a shared tumor microenvironment *in vivo*. Thus, the observed phenotypic effects of OTUB2 depletion may not fully represent the complex biology of coexisting tumors. Third, our bioinformatic analyses relied partly on public databases such as TCGA, which primarily contains genomic data on PTC but lacks comprehensive information on MTC and especially TCTs. This limits the ability to contextualize our mutational findings within a broader cohort of collision tumors and may affect the generalizability of the identified genetic signatures. Together, these constraints highlight the need for multi-center collaborations, more sophisticated co-culture or patient-derived xenograft models, and expanded genomic resources to further validate and extend the conclusions drawn here.

6. Conclusion

TCT is an uncommon occurrence in which distinct types of thyroid cancers coexist without intermingling. The most aggressive and poorest prognosis was observed with the coexistence of PTC and OTC. Our research is pioneers the use of whole-exome sequencing to investigate gene variations in a Chinese patient, revealing the heterogeneity of TCT and confirming that HRAS and STAG2 were the driver genes, while the deletion mutation OTUB2 was considered involved in the cancer proliferation of TCTs, and contributing to a poor outcome. This research effort faced challenges, such as the limited availability of samples due to the rarity of TCTs, the complexity of tumors interactions, technological constraints in advanced genetic analysis, and a gap in translating laboratory findings to clinical practice. In summary, our work positions OTUB2 as a relevant molecular player in thyroid cancer progression and suggests that its depletion can enhance malignant phenotypes. Further investigation into the mutation spectrum and functional consequences of OTUB2 alterations in clinical cohorts may help stratify patients and identify novel therapeutic vulnerabilities in thyroid malignancies.

Availability of Data and Materials

The raw sequence data reported in this study have been deposited in the Genome Sequence Archive (Genomics, Proteomics & Bioinformatics 2021) in the National Genomics Data Center (Nucleic Acids Res 2022), China National Center for Bioinformation/Beijing Institute of Genomics, Chinese Academy of Sciences (GSA-Human: HRA006138), which are publicly accessible at https://ngdc.cncb.ac.cn/gsa-human. The other datasets used or analyzed during the current study are available from the corresponding author on reasonable request.

Author Contributions

Conceptualization, YX, ML and QL; original draft preparation and editing, YX and ML; visualization, YX and QL; supervision and writing, YX and ML. Each author has participated sufficiently in the study. YX and QL were both the first authors, while YX and ML were both the corresponding authors. All authors contributed to editorial changes in the manuscript. All authors read and approved the final manuscript. All authors agreed to be accountable for all aspects of the work.

Ethics Approval and Consent to Participate

Written informed consent was obtained from the patient for publication of this case report and any accompanying images. This study was approved by the research ethics committee of Shandong Provincial Third Hospital (MR-37-23-052242) and certifies that it was performed in accordance with the ethical standards as laid down in the 1964 Declaration of Helsinki and its later amendments, or comparable ethical standards. Moreover, the ethical number of animal was DWSY-G2024005, which was approved by Shandong provincial third hospital animal committee. This study was carried out in accordance with the ARRIVE guidelines.

Acknowledgment

Thanks for the PPI network analysis from Guangchao Luan, who works at Jinan Third Hospital. And Thanks for the PCR-Sanger sequence from Fabao Liu who is a professor at Shandong University.

Funding

(1) Science and Technology Department of the National Administration of Traditional Chinese Medicine Joint Science and Technology Construction Project (GZY-KJS-SD-2024-063). (2) Joint Research Fund Project of Shandong Provincial Third Hospital and Shandong University Qilu Medical College (LHXM2024MS12001). (3) Shandong Provincial Third Hospital - Provincial Key Clinical Specialty in 2025 (SJZK202501). (4) Jinan City Science and Technology Plan - Medical Science and Technology Innovation Project (202430019).

Conflict of Interest

The authors declare no conflict of interest.

Declaration of AI and AI-Assisted Technologies in the Writing Process

In the preparation of this manuscript, the graphical abstract was created using an AI-based image generation tool (https://jova.ai/ai-image-generator). The AI tool was used solely for visual conceptualization and illustration purposes. All scientific content, data interpretation, and conclusions remain the sole responsibility of the authors. The

use of AI-generated images does not affect the originality, integrity, or scientific validity of the research presented.

Supplementary Material

Supplementary material associated with this article can be found, in the online version, at https://doi.org/10.31083/FBL49970.

References

[1] Bojoga A, Stănescu L, Badiu C. Collision tumors of the thyroid. A special clinical and pathological entity. Archive of Clinical Cases. 2021; 8: 84–90. https://doi.org/10.22551/2021.33.0804.10191.

[2] Abdullah AM, Qaradakhy AJ, Ahmed MM, Salih AM, Omar SS, Kakamad FH, *et al*. Thyroid collision tumors; A case series with literature review. Annals of Medicine and Surgery (2012). 2022; 76: 103444. https://doi.org/10.1016/j.amsu.2022.103444.

[3] Alzumaili B, Sadow PM. Update on Molecular Diagnostics in Thyroid Pathology: A Review. Genes. 2023; 14: 1314. https://doi.org/10.3390/genes14071314.

[4] Kim M, Kim BH. Current Guidelines for Management of Medullary Thyroid Carcinoma. Endocrinology and Metabolism (Seoul, Korea). 2021; 36: 514–524. https://doi.org/10.3803/EnM.2021.1082.

[5] Fugazzola L. Medullary thyroid cancer - An update. Best Practice & Research. Clinical Endocrinology & Metabolism. 2023; 37: 101655. https://doi.org/10.1016/j.beem.2022.101655.

[6] Censi S, Manso J, Mian C. Other markers of medullary thyroid cancer, not only calcitonin. European Journal of Endocrinology. 2023; 188: R1–R4. https://doi.org/10.1093/ejendo/lvac009.

[7] Harms PW, Frankel TL, Moutafi M, Rao A, Rimm DL, Taube JM, *et al*. Multiplex Immunohistochemistry and Immunofluorescence: A Practical Update for Pathologists. Modern Pathology: an Official Journal of the United States and Canadian Academy of Pathology, Inc. 2023; 36: 100197. https://doi.org/10.1016/j.modpat.2023.100197.

[8] Coffey AJ, Kokocinski F, Calafato MS, Scott CE, Palta P, Drury E, *et al*. The GENCODE exome: sequencing the complete human exome. European Journal of Human Genetics: EJHG. 2011; 19: 827–831. https://doi.org/10.1038/ejhg.2011.28.

[9] Li H, Handsaker B, Wysoker A, Fennell T, Ruan J, Homer N, *et al*. The Sequence Alignment/Map format and SAMtools. Bioinformatics (Oxford, England). 2009; 25: 2078–2079. https://doi.org/10.1093/bioinformatics/btp352.

[10] Wang K, Li M, Hakonarson H. ANNOVAR: functional annotation of genetic variants from high-throughput sequencing data. Nucleic Acids Research. 2010; 38: e164. https://doi.org/10.1093/nar/gkq603.

[11] Kanehisa M, Goto S. KEGG: kyoto encyclopedia of genes and genomes. Nucleic Acids Research. 2000; 28: 27–30. https://doi.org/10.1093/nar/28.1.27.

[12] Kawasaki K, Kai K, Tanaka N, Kido S, Ibi A, Minesaki A, *et al*. Collision tumor of a papillary and follicular thyroid carcinoma: a case report. Thyroid Research. 2023; 16: 24. https://doi.org/10.1186/s13044-023-00167-3.

[13] Toyoshima MTK, Domingues RB, Soares IC, Danilovic DLS, Amorim LC, Cavalcante ERC, *et al*. Thyroid collision tumor containing oncocytic carcinoma, classical and hobnail variants of papillary carcinoma and areas of poorly differentiated carcinoma. Archives of Endocrinology and Metabolism. 2021; 65: 495–499. https://doi.org/10.20945/2359-3997000000389.

[14] Tounsi Guettiti H, Traina H, Ben Ayed I, Ben Jemii N, Boubaker S, Alrageeg M, *et al*. BRAF V600E and Novel Somatic Mutations in Thyroid Cancer of Libyan Patients. Asian Pacific Journal of Cancer Prevention: APJCP. 2022; 23: 4029–4037. https://doi.org/10.31557/APJCP.2022.23.12.4029.

[15] Reagh J, Bullock M, Andrici J, Turchini J, Sioson L, Clarkson A, *et al*. NRASQ61R Mutation-specific Immunohistochemistry Also Identifies the HRASQ61R Mutation in Medullary Thyroid Cancer and May Have a Role in Triaging Genetic Testing for MEN2. The American Journal of Surgical Pathology. 2017; 41: 75–81. https://doi.org/10.1097/PAS.0000000000000740.

[16] Jagadeeshan S, Prasad M, Badarni M, Ben-Lulu T, Liju VB, Mathukkada S, *et al*. Mutated HRAS Activates YAP1-AXL Signaling to Drive Metastasis of Head and Neck Cancer. Cancer Research. 2023; 83: 1031–1047. https://doi.org/10.1158/0008-5472.CAN-22-2586.

[17] Pan Y, Gu Y, Liu T, Zhang Q, Yang F, Duan L, *et al*. Epitranscriptic regulation of *HRAS* by N^6-methyladenosine drives tumor progression. Proceedings of the National Academy of Sciences of the United States of America. 2023; 120: e2302291120. https://doi.org/10.1073/pnas.2302291120.

[18] Ma Y, Sun Y. miR-29a-3p inhibits growth, proliferation, and invasion of papillary thyroid carcinoma by suppressing NF-κB signaling via direct targeting of OTUB2. Cancer Management and Research. 2019; 11: 13–23. https://doi.org/10.2147/CMAR.S184781.

[19] Li Y, Chen X, Xu X, Chen C, Min M, Liang D, *et al*. OTUB2 contributes to vascular calcification in chronic kidney disease via the YAP-mediated transcription of PFKFB3. Theranostics. 2025; 15: 1185–1204. https://doi.org/10.7150/thno.98660.

[20] Mei F, Deng D, Cao Z, Lou L, Chen K, Hu M, *et al*. Deubiquitination of RIPK3 by OTUB2 potentiates neuronal necroptosis after ischemic stroke. EMBO Molecular Medicine. 2025; 17: 679–695. https://doi.org/10.1038/s44321-025-00206-6.

[21] Mao JT, Xue B, Lu QY, Lundmark L, Burns W, Yang J, *et al*. Combinations of grape seed procyanidin extract and milk thistle silymarin extract against lung cancer - The role of MiR-663a and FHIT. Life Sciences. 2023; 318: 121492. https://doi.org/10.1016/j.lfs.2023.121492.

[22] Zhang C, Chen B, Jiao A, Li F, Sun N, Zhang G, *et al*. miR-663a inhibits tumor growth and invasion by regulating TGF-β1 in hepatocellular carcinoma. BMC Cancer. 2018; 18: 1179. https://doi.org/10.1186/s12885-018-5016-z.

[23] Wang G, Chen L, Jian W, Fang L. Low Expression of miR-663a Indicates Poor Prognosis and Promotes Cell Proliferation, Migration, and Invasion in Breast Cancer. Oncology Research and Treatment. 2021; 1–8. https://doi.org/10.1159/000513405.

[24] Zhou L, Pan X, Li Z, Chen P, Quan J, Lin C, *et al*. Oncogenic miR-663a is associated with cellular function and poor prognosis in renal cell carcinoma. Biomedicine & Pharmacotherapy. 2018; 105: 1155–1163. https://doi.org/10.1016/j.biopha.2018.05.082.

[25] Zhao S, Xiong W, Xu K. MiR-663a, regulated by lncRNA GAS5, contributes to osteosarcoma development through targeting MYL9. Human & Experimental Toxicology. 2020; 39: 1607–1618. https://doi.org/10.1177/0960327120937330.

[26] Qiu YU, Liu R, Huang S, Cai Q, Xie YI, He Z, *et al*. OTUB2 promotes proliferation and metastasis of triple-negative breast cancer by deubiquitinating TRAF6. Oncology Research. 2025; 33: 1135–1147. https://doi.org/10.32604/or.2025.062767.

[27] Xu X, Wu G, Han K, Cui X, Feng Y, Mei X, *et al*. Inhibition of OTUB2 suppresses colorectal cancer cell growth by regulating β-Catenin signaling. American Journal of Cancer Research. 2023; 13: 5382–5393.

[28] Xu L, Wang B, Gang Z, Han Z, Wang A, Liu Q, *et al*. Ubiquitin-conjugating enzyme E2S decreases the sensitivity of glioblastoma cells to temozolomide by upregulating PGAM1 via the interaction with OTUB2. International Journal of Biological Macromolecules. 2025; 302: 140583. https://doi.org/10.1016/j.ijbiomac.2025.140583.

[29] Wu Y, Mohd Sani SB, Peng K, Lin T, Tan C, Huang X, *et al*. Research progress of the Otubains subfamily in hepatocellular carcinoma. Biomedicine & Pharmacotherapy. 2024; 179: 117348. https://doi.org/10.1016/j.biopha.2024.117348.